frontiers | Frontiers in Marine Science

TYPE Original Research
PUBLISHED 08 February 2023
DOI 10.3389/fmars.2022.1085142

OPEN ACCESS

EDITED BY
Wen Zhuang,
Shandong University, China

REVIEWED BY
Chuanbo Guo,
Institute of Hydrobiology (CAS), China
Fajin Chen,
Guangdong Ocean University, China

*CORRESPONDENCE
Kai Liu
kliu@yic.ac.cn

SPECIALTY SECTION
This article was submitted to Marine Biogeochemistry, a section of the journal Frontiers in Marine Science

RECEIVED 31 October 2022
ACCEPTED 13 December 2022
PUBLISHED 08 February 2023

CITATION
Ren P, Schmidt BV, Liu Q, Wang S, Liu X, Liu K and Shi D (2023) Fractionation of toxic metal Pb from truly dissolved and colloidal phases of seaward rivers in a coastal delta. *Front. Mar. Sci.* 9:1085142. doi: 10.3389/fmars.2022.1085142

Fractionation of toxic metal Pb from truly dissolved and colloidal phases of seaward rivers in a coastal delta

Peng Ren[1], Bjorn V. Schmidt[2], Qun Liu[3], Shuzhen Wang[4], Xinyan Liu[5], Kai Liu[1,6*] and Dalei Shi[1]

[1]Dongying Research Institute for Oceanography Development, Dongying, Shandong, China, [2]Department of Biological and Environmental Sciences, Texas A&M University-Commerce, Commerce, TX, United States, [3]Bureau of Agriculture and Rural Affairs of GuangRao, Dongying, Shandong, China, [4]Dongying Real Estate Registration Center Dongying Branch, Dongying, Shandong, China, [5]Natural Resources and Planning Bureau of Lijin, Dongying, Shandong, China, [6]China University of Petroleum, National University Science and Technology Park Postdoctoral Workstation, Dongying, Shandong, China

Colloids of natural river water is a key intermediate carrier of lead (Pb). It is important to monitor the transport–transformation behavior of Pb in the colloidal phase of seaward water because this behavior is related to the levels of pollution input and environmental risks posed to the sea, especially in coastal delta areas. In this study, the fractionation behavior and distribution of toxic Pb from the truly dissolved phase and the different colloidal phases in seven seaward rivers in the Yellow River Delta were investigated. The concentrations of total dissolved Pb, truly dissolved Pb, and colloidal Pb were 0.99–40.09 μg L^{-1}, 0.40–8.10 μg L^{-1}, and 0.60–35.88 μg L^{-1}, respectively. In freshwater rivers, the main component of total dissolved Pb (about > 50%) is truly dissolved Pb but the main component of total dissolved Pb in the seawater environment is colloidal Pb (> 80%). A dramatic increase in salinity causes the deposition (about ≈94%) of all forms of Pb to sediment from estuarine water in winter. However, this sedimentation behavior of colloidal Pb gradually decreases (in the Shenxiangou River) when the river salinity approaches seawater salinity (S = ≈29). In the industrial port (Xiaoqinghe River) and mariculture (Yongfenghe River) estuarine areas, which have extensive seawater, the deposition behavior of colloidal Pb (<15%) is less affected by the change in salinity. This suggests that human activity contributes to the spread of Pb in the offshore environment. The concentration of 100 kDa–0.22 μm Pb has a postive correlation with total colloidal Pb. Its variation is minimally affected by salinity compared with other colloidal components. In addition, the correlation between the molecular weight and aromaticity of chromophoric dissolved organic matter (CDOM) and colloidal Pb suggests that macromolecules in seawater will be important transport carriers of Pb. In all, truly dissolved Pb is the main transport form of dissolved Pb in river freshwater; however, in brackish water in estuaries, colloidal matter gradually becomes the

main transport carrier. Surging salinity immobilizes truly dissolved Pb in the estuarine region, but colloidal matter inhibits this deposition. Colloidal phase is the important conversion for land–sea transport of Pb by seaward rivers.

KEYWORDS

metal fractionation, colloidal components, salinity deposition, truly dissolved, migration behavior

1 Introduction

Heavy metals pose a very serious health risk for humans and wildlife because of their biological toxicity, carcinogenic effects, and ability to bioaccumulate in food chains (Huang et al., 2011; Latosinska and Czapik, 2020; Men et al., 2020; Xiang et al., 2021). These risks are mainly dominated by metal speciation and existence in the environment (Weng et al., 2014). Previous studies have shown that free heavy metal ions have significantly higher toxicity and form deposits more easily because of their higher redox potential (Dallas et al., 2013). However, macromolecular organic compounds (>1 kDa, kilodalton), including natural colloidal organic matter, could complex the structure of the free metal ions, and their ability to form deposits (Fytianos, 2001). Natural aqueous environments, such as rivers, seas, and lakes, could supply abundant natural macromolecular organic matter (the main components of natural organic matter) to complex the free metal ions' structure, and their ability to form deposits (Fytianos, 2001). Furthermore, colloidal organic matter (COM) rich in hydroxyl functional groups, tends to make the bound metal more lipid-soluble, which enhances its bioavailability for metals such as lead (Pb), mercury (Hg_3), and antimony (Sb_{51}) (Hargreaves et al., 2018). This could have a profound impact on the migration and conversion behaviors of heavy metals in river environments (He et al., 2016). However, emphasizing the diverse effects of these factors, colloidal organic matter, which is mainly composed of humic acid, often also plays a role in reducing metal toxicity. In addition, colloidal organic matter can modify the surface properties of particles to facilitate or hinder their adsorption of metal ions (Liu and Gao, 2019). Therefore, it is necessary to investigate the geochemical behavior between heavy metals with natural colloidal organic matter in natural water systems.

Lead (Pb), is widely used in natural water environments and, therefore, is a reliable indicator of human activity in these environments, and is a compound that has a unique geochemical behavior (Zhang et al., 2008). Pb ions typically have high exhibit biotoxicity, they easily form sediments, and are difficult to release from mineral and particulate states (Savenko and Savenko, 2019). However, natural organic matter (mainly colloidal organic matter) has a strong complexing effect on Pb ions and facilitates Pb migration and release. It has been demonstrated that colloidal organic matter can prevent the formation of low-solubility mineral lead, such as cerussite and hydrocerussite crystals, and enhance the formation of soluble lead ions (Abdelrady et al., 2021). The chromophoric dissolved organic matter (CDOM), which is an important component of colloidal matter, could be the key factor to influence the geochemical behavior of Pb (Stolpe and Hassellov, 2010). The CDOM-complex-Pb could directly contact plasma membranes of organisms by adsorption and express a higher biological risk than free ions, ultimately (Nadella et al., 2013; Worms et al., 2015). However, environmental conditions, such as the pH value of seawater (i.e., seawater acidification), are important factors that affect the distribution of heavy metals in different phases (Lao et al., 2019; Ma et al., 2019; Lao et al., 2022). Under the influence of salinity and pH, the binding ability of different components of CDOM to Pb varies greatly (Wood et al., 2011). Furthermore, the change of physicochemical factors also affects the molecular structure of the CDOM (Guzman et al., 2014), which in turn affects the formation of complex bonds between CDOM and metal ions (Liu et al., 2019). This biogeochemical process is key factor to affect the environment risk of Pb in the environment which salinity and pH changed dramaticly (Marcinek et al., 2022). In all, the transformation to the colloidal phase is a very important aspect of the geochemical cycle of Pb in natural water systems.

River water flowing into the sea is the most important transportation and conversion channel for Pb in the natural environment, especially in coastal deltas. Pb enters offshore waters as part of the river flow, in turn having toxicological effects on marine organisms such as plankton, urchin and fish (Cao et al., 2018). Meanwhile, these rivers tend to vary drastically in salinity, which could have a profound effect on the interaction between CDOM and Pb (Marcinek et al., 2022). It is important to monitor the concentration, distribution, and sources of Pb in rivers flowing into sea. The Yellow River Delta is a typical wetland ecosystem in a warm, temperate zone of the world. Unlike the Pearl River and the Yangtze River deltas, which have highly developed industries, there are several unique features

pertaining to the industrial and economic development in this region. This region comprises a highly developed chemical industry in a narrowly confined space, an undeveloped nature reserve, and regions with primarily agricultural and maricultural developments (Zhi et al., 2020). These areas are closely linked through a dense network of rivers in the delta. Some rivers also serve at the same time as a source of water and a sewage ditch (Cheng et al., 2021). These rivers are the primary transportation and conversion channels through which Pb enters Laizhou Bay. As the fastest hydrodynamic exchange (0.52a) area within the Bohai Sea, Laizhou Bay could potentially spread Pb to the Bohai Sea and even to the Yellow Sea (Lin et al., 2019). Recently, the pollution control required in the Yellow River Delta and the Bohai Sea has received unprecedented attention from the Chinese government (Ma et al., 2019). It is essential to monitor the ecological risk speciation of Pb in the rivers flowing into sea in these deltas. Analysis of colloidal Pb in the rivers would provide essential evidence for evaluating the environmental risks posed by pollution in the Bohai Sea and the Yellow River Delta.

In this study, the distribution and fractionation of Pb at different stages of the colloidal phase (<1 kDa, 1–3 kDa, 3–10 kDa, 10–100 kDa and 100 kDa–0.22 μm) in six seaward rivers of the Yellow River Delta in winter were investigated. The six rivers pass through urban, industrial, mariculture, and agricultural areas located in the south and northeast region of the Yellow River Delta. There are two main rivers (the Yellow River and Xiaoqinghe River), and four canals driven by the Yellow River: Yongfenghe River, Guangli River, Xiaodaohe River and Shenxiangou River. We selected winter as the period to study the fractionation of the toxic metal Pb in the colloids. In this season, the change of colloidal properties is slow because of the lower winter temperatures, which could prolong the interaction time between Pb and colloidal matter (Wu et al, 2020; Mudge et al., 2021).

2 Materials and methods

2.1 Reagents and labware preparation

In this study, the maximum experimental safe gap must be minimized because there are trace levels of Pb in the Yellow River (Gao et al., 2015). All reagents used in this study were guaranteed reagent (GR) grade. The concentrated form of nitric acid (HNO_3) (Fisher®) used in this study was distilled by an acid purification system (DST-4000, Savillex™). The stock solution of 1 mg L^{-1} Pb was prepared in 10% HNO_3 (v/v) by multistage dilution. The 1000 mg L^{-1} standard solution was prepared in 500 mL of polytetrafluoroethylene bottles (Asone®). The Pb standard solution was Cl-forms (+2) and was supplied by the National Center of Analysis and Testing for Nonferrous Metals and Electronic Materials, China. Ultrapure water (>18 MΩ-cm) was obtained by a water purification system (Milli-Q®).

The labware, including sampling bottles and tubes, had to be made from Teflon materials (Teflon®) and cleaned according to a strict trace metal cleaning process (Liu et al., 2018). First, a pre-cleaning process was conducted to wash away obvious dirt from the labware, with tap water, 10% cleaning solution (v/v) (Decon90®), and ultrapure water (>18 MΩ-cm), being used successively. Second, the pre-cleaned labware was soaked in 10% hydrochloric acid (HCL) (v/v) (Fisher®) and 3% HNO_3 (v/v) for 48 h, respectively. Ultrapure water was used to rinse residual acid off the soaked labware; this was performed five times. Finally, labware were dried in the ultra-clean bench (Class 100) at room temperature (i.e., 20–25°C). After drying, each piece of labware was double-bagged in polyethylene Ziploc (Ziploc®) bags and stored in a sealed container at a consistent temperature range of 20–25°C.

2.2 Sampling collection

The study areas were in the Yellow River Delta, which is a typical wetland ecosystem in a warm, temperate zone of the world (Figure 1). Sampling stations were selected according to the locations of cities, villages, farmlands, industrial areas, breeding areas, and salt fields that the seaward rivers passed through during January 2020 (Figure 1). Surface water samples (10–20 cm) were collected and the clean sampling system was used according to the trace metal rule to avoid contamination at all stations. The clean sampling system is composed of a desktop ultra-clean workbench, peristaltic pump, water intake system, syringe filter, and a sampling bottle (Li et al., 2015; Liu et al., 2018). All sample components were connected by C-Flex tubes. The sample process is briefly described below (Figure 2A). First, the water intake system was washed five times with ultrapure water before sampling. Second, the pre-washed water intake system was placed 10–20 cm below the surface at the sample water station. Third, the peristaltic pump (Masterflex®) was turned on so that the water sample passed through the syringe filter (Swinnex®) with the pre-installed membrane (0.22 μm; Pall®). The first 10 mL of sample was discarded to prevent interference from the membrane. A total volume of 1 L of the water sample was collected into the fluorinated high-density polyethylene sample bottle (Nalgene®), after which 1 mL of concentrated HNO_3 was added and the sample stored at room temperature. The other 1 L of water was collected in the fluorinated high-density polyethylene sample bottle and metal was separated by ultrafiltration as soon as possible in the laboratory (<48 h). A total of 70 mL of water sample was taken in a brown glass bottle for DOC and CDOM analysis (<48 h). Further steps were required. The water intake system

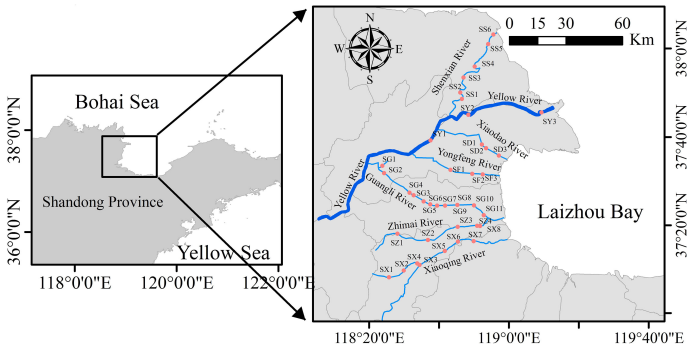

FIGURE 1
Location map of sampling stations in seaward rivers in the Yellow River Delta. The blue dots indicate sampling sites, and the blue line represents the river.

should be soaked in 3% HNO_3 (v/v) until just before use. The filter membrane should be replaced after the filtration of every sample. The basic hydrological data, such as salinity, pH, and temperature, were measured by the multiparameter water quality analyzer (YSI®).

2.3 Colloidal Pb fractionation

The different sizes of colloidal Pb were separated according to centrifugal ultrafiltration (CUF) units (Amicon® Ultra-15) using a fixed-rotor centrifuge (Cence®). Four cut-off values (i.e., <1 kDa,<3 kDa,<10 kDa,<100 kDa) of CUF units were used. The ultrafiltration process is as follows (Figure 2B). First, the CUF units were sequentially washed 6–8 times with 0.1% sodium hydroxide (NaOH) (g/g), 0.06% HCl (v/v), and ultrapure water to remove possible contaminants (Lu et al., 2020). Second, 15 mL of sample was loaded to the obtain the different cut-off values and centrifuged for 50–70 min at 4800×g in the rotor centrifuge. Approximately 0.5 mL of ultrafiltrate was obtained from the inner ultrafiltration tube and transferred to the pre-cleaned 10-mL polypropylene sample centrifuge tube (Falcon™). After CUF, 1 mL of 3% HNO_3 (v/v) was added to the inner tube and soaked for 2 h to extract the residual colloidal metal. The extraction was performed three times and mixed in the sample tube. The volume of colloidal sample was adjusted to 5 mL with 3% HNO_3 (v/v). Before measuring, colloidal Pb samples were stored in an ultra-clean bench (Class 100; at 25°C) for more than 1 week to ensure that the colloidal organic matter was fully decomposed. Finally, 0.2 mL of the decomposed solution was diluted to 10 mL with 3% HNO_3 (v/v); this solution was then used for detecting colloidal Pb.

A method blank and solvent blank of the ultrafiltration were used simultaneously with samples to assess errors. It should be noted that the actual cut-off values of the CUF used in this experiment were generally higher than those stated by the

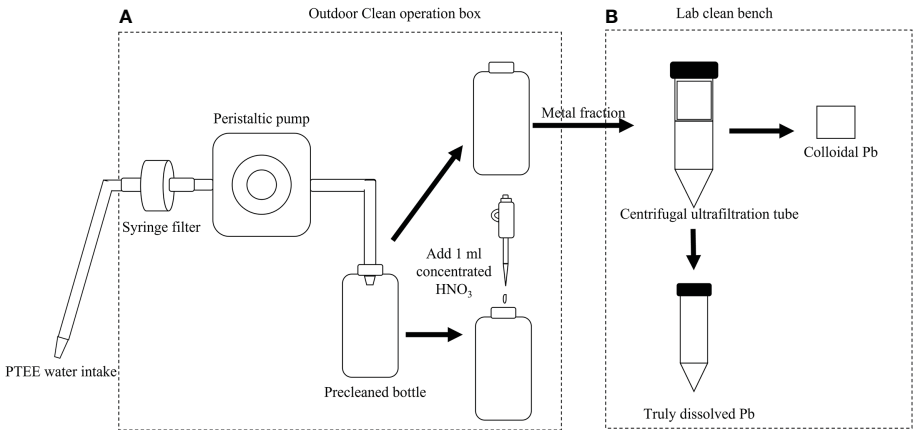

FIGURE 2
The diagram of clean sampling and metal fractionation. **(A)** The clean sampling process; and **(B)** the metal fractionation process.

manufacturer (Xu et al., 2018; Lu et al., 2020). This can usually lead to biased perceptions of the colloidal trace element concentration in the ultrafiltrate by researchers. We used standard macromolecules, including vitamin B_{12} and standard fluorescent-tagged dextrans, to calibrate the CUF units according to previous studies (Lu et al., 2019; Lu et al., 2020).

2.4 Fractionation factor

The fractionation factor (F) was defined as the ratio of the concentration of truly dissolved Pb and colloidal Pb to evaluate the fractionation behavior of Pb by the colloids present in the system (Liu et al., 2019):

$$Fclt = \frac{C_{Pb,c}}{C_{Pb,t}}$$

where $C_{Pb3,c}$ and $C_{Pb3,t}$ are the concentrations of Pb in colloids, respectively. $F_{c/t}$ is the fractionation factor between colloidal Pb and truly dissolved Pb. When the $F_{c/t} > 1$ or< 1, the Pb preferentially migrated to colloidal matter or the truly dissolved phase.

2.5 Chromophoric dissolved organic matter

The UV absorption spectrum of CDOM was measured using a UV–Vis spectrophotometer (TU-1950, Persee®). Ultrapure water was used as a blank and for baseline scanning. The samples were spectrally scanned in the range of 200–800 nm, and the scanning interval was 1 nm. All absorbance values were deducted by the mean value of the 680–700 nm range to eliminate the refractive index differences and baseline drift.

The absorption coefficient $a(355)$ was selected as the parameter represent the concentration of CDOM and was calculated from the following equation (Peuravuori and Pihlaja, 1997; Wu et al., 2022):

$$a(\lambda) = 2.303xA(\lambda)/L$$

where $a(\lambda)$ (m^{-1}) is the absorption spectrum at the wavelength of λ nm; $A(\lambda)$ is the absorbance at the wavelength of λ nm; and L is the length of cuvette.

The specific ultraviolet absorbance ($SUVA_{254}$) was defined as the ratio of the absorption coefficient at the wavelength of 254 nm to the concentration of dissolved organic matter (DOC) of the sample. This parameter could represent the aromaticity of CDOM in the aquatic system. It was calculated from the following equation (Peuravuori and Pihlaja, 1997; Wu et al., 2022):

$$SUVA_{254} = \frac{a(254)}{C_{DOC}}$$

where $SUVA_{254}$ (l (mg m)$^{-1}$) is the specific ultraviolet absorbance; $a(254)$ is the absorption spectrum at the wavelength of 254 nm; and C_{DOC} is the concentration of dissolved organic matter.

The ratio of the absorption coefficient (E2 : E3) at a specific wavelength was used to represent the change of the relative molecular weight of CDOM and was calculated using the following equation (Peuravuori and Pihlaja, 1997; Wu et al., 2022):

$$\frac{E_2}{E_3} = \frac{a(250)}{a(365)}$$

where E_2/E_3 is the ratio of the absorption coefficient of the water sample at the wavelength of 250 and 365 nm; $a(250)$ is the absorption coefficient at the wavelength of 250 nm; and $a(365)$ is the absorption coefficient at the wavelength of 365 nm.

2.6 Instruments and analysis

In this study, the concentration of different sized colloidal Pb was determined by using an inductively coupled plasma mass spectrometer (ICP-MS, iCAP RQ, Thermo Fisher Scientific Inc). The internal standard [indium (In_{49}), 10.00 μg^{-1}] was spiked in every sample. To maintain the stability of the instrument, we used 1.00 μg L^{-1} tune solution [lithium (Li_3), cerium (Ce_{58}), barium (Ba_{56}), In_{49}, and uranium (U_{92})] to monitor the oxide formation (BaO/Ba< 3%). The isobaric interference on Pb was corrected by monitoring ^{200}Hg and ^{111}Cd (Cd_{48}). The data of ^{108}Pb, ^{65}Cu (Cu_{29}), ^{68}Zn (Zn_{30}), ^{85}Sr (Sr_{38}), ^{89}Y (Y_{39}), and ^{95}Mo (Mo_{42}) were used to monitor the potential polyatomic interference. ICP-MS analysis was conducted with 99.999% argon at the optimized plasma gas flow rate (GFR) of 15.0 L min^{-1}, an auxiliary GFR of 1.2 L min^{-1} and at a nebulizer GFR of 0.88 L min^{-1}.

To ensure the accuracy of the method, we measured the method blanks to verify and control the reliability of the analysis data. The method blanks were determined by using an ultrapure water sample. The method blank followed the same process as sample preparation as follows: 3% HNO_3 extraction, 3% HNO_3 dilution, and ICP-MS parallel determination (n = 11) (Lu et al., 2020). The quantification limits [i.e., limit of quantification (LOQ)] for Pb were 10 times that of the standard deviation (σ) of the blanks, and the detection limits [i.e., limit of detection (LOD)] were 3σ (Table 1). To verify LOQ and LOD, we used the GBW08608 and GSB07–1183 reference materials to test the linear correlations (R^2) of the method. The linear ranges were 0.2 μg L^{-1}, 0.5 μg L^{-1}, 1 μg L^{-1}, and 2 μg L^{-1}. The performance was shown in Table 1. 0.50 μg L^{-1} of Pb standard sample was determined every 12 samples to measure the stability of the ICP-MS.

ICP–MS, inductively coupled plasma mass spectrometer; LOD, limit of detection; LOQ, limit of quantification.

TABLE 1 Performance of the inductively coupled plasma mass spectrometer (ICP-MS) and the analysis method.

	LOD (μg L^{-1})	LOQ (μg L^{-1})	Linear ranges (μg L^{-1})	Linear correlations (R^2)
Analysis method	0.14	0.43	–	–
GBW08608	–	–	0.2–2	0.9999
GSB07–1183	–	–	0.2–2	0.9999

–, represents no data.

3 Results

3.1 Mass balance, the actual cutoff of centrifugal ultrafiltration

The fractionation method, solvent used, and detection error will determine the result of Pb in the different samples. We used the mass balance (M) to monitor the precision of the result. The mass balance was defined as the ratio between the dissolved concentration of Pb of the non-fractionated sample and the summary of the different fractionation concentrations of Pb. Once the difference value between M and 100% was less than 10%, we believe that there on loss during the experiment. Moreover, once the value reached greater than 10%, we believed that the loss of Pb affects the result of the experiment (Liu and Gao, 2019). The mass balance ratio results of the different stations are shown in Figure 3. The mass balance ratio difference between M and 100% was 9%–10%. This means that the level of error introduced by the method, solvent and detection was overlooked in this study. Notably, the recovery ratio varied with the location of the sample station. Higher recovery ratios were observed in stations influenced by human activities. It is shown that there is an inference relationship between human activities and Pb. Intense human activity often leads to a stronger release of Pb into the environment (Zang et al., 2020). It will lead to the introduction of Pb contamination during field sampling or pre-treatment, ultimately causing high recovery rates (Chen et al., 2022).

The actual cut-off value for CUF was consistent with previous work because we used the same batch of products in this study (Liu et al., 2018; Lu et al., 2019; Lu et al., 2020). The actual MWCO of the 1, 3, 10 and 100 kDa CUF units were estimated to be 2, 7, 32 and 393 kDa, respectively. This indicated an overestimation of the colloidal trace element concentration in the ultrafiltrate of this study. However, the ultrafiltration performance of the CUF could still precisely fractionate the Pb into different sized colloids. Therefore, the experimental results could reflect the migration behavior of Pb from truly dissolved to colloidal phases in rivers flowing into sea.

3.2 Hydrographic parameters

Hydrographic parameters such as water temperature, salinity and pH of the rivers are described in Table 2. Water temperature of all the stations fluctuated in the range of 1.6°C to 7.8°C, with gradual decreases toward the direction of input sea. In addition, more than 80% stations were lower than 5°C, which

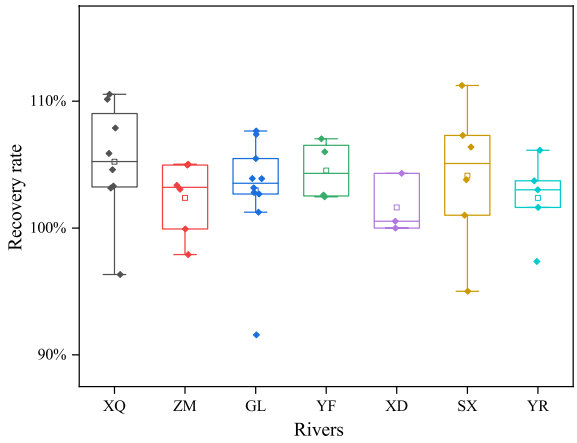

FIGURE 3
The mass balance of lead (Pb) in different rivers. XQ represents the Xiaoqinghe River; ZM represents the Zhimaihe River; GL represents the Guanglihe River; YF represents the Yongfenghe River; XD represents the Xiaodaohe River; SX represents the Shenxiangou River; and YR represents the Yellow River.

10.3389/fmars.2022.1085142

TABLE 2 Hydrographic parameters, such as water temperature, salinity, and pH of the rivers.

Sample station	Temperature (°C)	pH	Salinity (S)
Yellow River			
SY1	2.7	8.71	0.42
SY2	2.4	8.71	0.42
SY3	1.8	8.84	0.42
Xiaoqinghe River			
SX1	6.0	8.29	1.2
SX2	5.8	8.28	1.21
SX3	7.8	8.17	2.67
SX4	6.8	8.32	2.08
SX5	5.5	8.43	1.88
SX6	5.3	8.36	2.13
SX7	4.8	8.42	2.10
SX8	3.7	8.30	7.70
Yongfenghe River			
SF1	1.6	8.62	9.42
SF2	2.6	8.52	9.09
SF3	2.2	8.44	15.38
Xiaodaohe River			
SD1	2.3	8.49	21.45
SD2	3.2	8.43	21.86
SD3	2.4	8.47	26.42
Zhimaihe River			
SZ1	3.5	8.32	4.33
SZ2	3.1	4.18	8.71
SZ3	3.9	7.83	8.57
SZ4	2.5	8.21	14.25
SZ5	2.4	8.29	17.20
Guanglihe River			
SG1	3.9	8.24	2.83
SG2	3.3	8.96	1.75
SG3	4.1	8.59	4.93
SG4	5.5	8.16	4.86
SG5	3.9	8.81	3.29
SG6	3.7	9.08	2.68
SG7	3.5	9.08	2.44
SG8	3.6	9.08	2.51

(Continued)

TABLE 2 Continued

Sample station	Temperature (°C)	pH	Salinity (S)
SG9	3.5	9.12	3.77
SG10	3.2	8.51	10.87
SG11	2.7	8.38	18.33
Shenxiangou River			
SS1	3.7	8.37	1.48
SS2	4.1	8.55	0.99
SS3	4.1	8.59	1.11
SS4	3.7	9.25	5.76
SS5	2.0	8.70	21.03
SS6	1.5	8.28	29.46

means that the biogeochemical effects between microorganisms and the metals were very small and could be negligible (Cao et al., 2018; Marcinek et al., 2022). A notable phenomenon was that the water temperature of the Zihe-Xiaoqinghe river system was significantly higher (i.e., ≈1°C) than that of other rivers in this study. Higher water temperatures (i.e., >5°C) were recorded at the station near the village and the highway. The pH of most rivers was above 8.10, and the highest value appeared at the station of Shenxiangou River, with a value of about 9.25 (Table 2). There is an obvious high pH (>9.00) area in the Guanglihe River section passing through the urban area of Dongying City (Figure 3). This higher pH may be related to the weak flow of the river and the salinization of the land. To prevent sea tide intrusion, the flow of the Guangli River into the sea is controlled by a dam with fixed opening and closing times. The damming of the river by humans leads to a weaker flow of the Guangli River. A weak Guanglihe River flow is susceptible to saline seepage from salinized sediment, which often increases the pH of the water (Xie et al., 2019). In addition, in the reach of the Zihe River (which merges into the Xiaoqinghe River), there are stations with pH lower than 8.00, with values around 7.70–7.90. The station with the lowest pH (≈4.18) appears in the Zhimaihe River section, close to an industrial area, and the low pH river section continues for about 15 kilometers. From the potential results, all rivers are reducing environments under alkaline conditions, with the river pH >7.00 (Table 2). Significant differences were found in the salinity of the rivers. For the main rivers, such as Yellow River and Xiaoqinghe River, changes of salinity were not detected owing to the impact of the strong supply of upstream fresh water. There is no significant change of the salinity at the stations of the Yellow River, which remained at 0.42. In the Xiaoqing River, whose hydrodynamic force is weaker than that of the Yellow River, the salinity only reaches 7.00 at the station near the estuary and did not exceed 3.00 at other stations. For the trunk channels, the salinity changed drastically. A pronounced increase of salinity was found along the direction of the seaward river output into the sea. Some sample stations with a salinity greater than 20.00 appeared in the Xiaodaohe River and Shenxiangou River. The salinity changes observed in the Guanglihe River and Yongfenghe River were relatively slow, but the salinity exceeds 15.00 at the stations near the estuary.

3.3 The concentration of Pb in the seaward river

The seaward rivers could be classified into three categories according to the discussion in Section 3.1. The Xiaoqinghe River and the Yellow River are natural rivers (NR). Trunk canals of the Yellow River are divided into two categories according to the influence of tidal seawater. The Yongfenghe River and Xiaodaohe River are rivers strongly influenced by seawater (SFR), whereas the Zhimaihe River, Guanglihe River, and Shenxiangou River are weakly influenced by seawater (WFR).

3.3.1 Total dissolved Pb

Total dissolved Pb is the sum of colloidal and dissolved lead, which reflects the level of transportable Pb in water. It is an important indicator for measuring Pb pollution in the river. The distribution of dissolved Pb in the different rivers was described in Figure 4. The concentration of total dissolved Pb in all rivers ranged from 0.99 to 40.09 μg L^{-1}. The concentration gradually decreased as the location approached the estuary and did not exceed the surface water standard for China (i.e., 100.00 μg L^{-1}) for more than 95% of the stations. Only three stations, SZ1, SX1, and SZ5, were observed with values over and above the standard. SZ1 had a concentration of 19.73 μg L^{-1} and was in the upstream sample area of the Xiaoqing River. SZ1 and SZ5 were all in the Zhimaihe rivers, with the concentrations of 40.09 μg L^{-1} and 12.94 μg L^{-1}, respectively. Among these sites, SX1 and SZ1 are

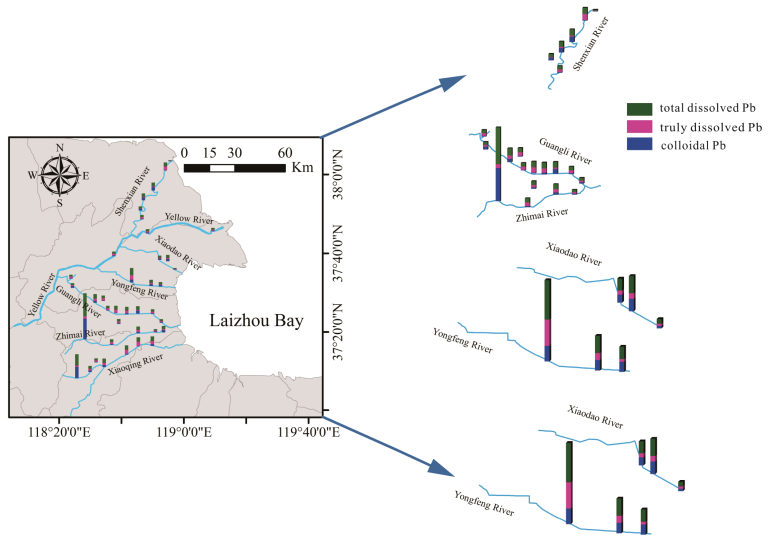

FIGURE 4
The distribution of total dissolved lead (Pb), truly dissolved Pb, and colloidal Pb in different seaward rivers.

the highest concentration points regarding concentrations of Pb and were also the farthest from the estuary along the river where they are located. However, SZ5 is near the estuary. The minimum concentration of total dissolved Pb occurred near the Shenxiangou estuary and was about 0.99 μg L^{-1}.

Obvious variations were found in the distribution trend of total dissolved Pb in different rivers. Among the five trunk canals of the Yellow River, the concentration of Pb decreased gradually with the increase of salinity in rivers, which was strongly influenced by seawater. But in other trunk canals, the distribution of Pb is relatively complex. A trough-like distribution trend of Pb was observed along the direction of the Zhimai River flowing into the sea. The highest fluctuation of about 35.00 μg L^{-1} Pb and a significant increment of about 10.50 μg L^{-1} of Pb was observed at the Zhimaihe estuary. In Shenxiangou and Guangli River, the distribution of Pb showed more frequent and smaller fluctuation changes (i.e., 0.20–5.70 μg L^{-1}). Those differences may be related to the river basin. The sampling areas of the Yongfenghe River and Xiaodaohe River are mostly surrounded by mariculture and salt-drying farms, the Guangli River and Shenxiangou flow through urban areas and townships, and the Zhimaihe River flows through farmland, industrial areas, and salt farms. The concentration of Pb in urban areas was higher than areas of farmland and salt farms. It should be noted that the hydrodynamic forces of these rivers are weaker than natural rivers. For the natural rivers, the distribution of Pb was also different. The concentration of Pb in the Xiaoqing River was significantly higher than that of the Yellow River, and with an average concentration difference of about 5.00 μg L^{-1}. In the Yellow River, the concentration variations in the different stations are lower, with a range of 0.50–1.5 μg L^{-1}. However, it could reach 16 concentration units in the stations of the Xiaoqinghe River. A gradual decrease of Pb concentration was observed as the location approached the estuary in the Yellow River. However, the Pb concentration increased significantly at the SY3. In the Xiaoqing River, the distribution trend of Pb was a mechanical wave like that observed in the Guangli River. A sharp decrease in Pb concentration was recorded at the upstream position of the sampling area (SX1→SX2). In addition, the Pb concentration increased at the junction area of the Zihe River with the Xiaoqinghe River. After the mixture, Pb concentration increased to 7.28 μg L^{-1} at SX3 station.

3.3.2 Truly dissolved Pb

Metal ions in true solution are very mobile and bioavailable Therefore, it is necessary to give a further explanation for the investigation of the geochemical behavior of Pb in the river. Truly dissolved Pb concentrations in the rivers varied with the location of the sample station (Figure 4). For all rivers, the concentration of truly dissolved Pb ranged from 0.25 to 7.37 μg L^{-1}. The highest concentration of truly dissolved Pb appeared at SF1 in the Yongfenghe River and the lowest appeared at SX1 in the Xiaoqing River. In the two natural rivers, truly dissolved Pb was the dominant fractionation (i.e., >60%) of the total dissolved Pb and ranged from 1.57 to 2.99 μg L^{-1}. For both rivers, following a downstream, seaward direction, truly dissolved Pb of the samples increased then declined. The average concentration of truly dissolved Pb in the Xiaoqing River was significantly higher than that in the Yellow River. In some river reaches of the Xiaoqing River, the truly dissolved Pb increased significantly to about 2.22 μg L^{-1}, especially for those sample

stations located in urban or farmland areas. The distribution trend of truly dissolved Pb varied across the trunk canals. A decrease of truly dissolved Pb was found in the SFR river as stations neared the estuary, with a sharp decline to about 4.68 μg L^{-1} observed in the Yongfenghe River. However, truly dissolved Pb demonstrated significant fluctuations in the TFR river. A pronounced increase in truly dissolved Pb was found in the Zhimai River estuary, which was a different pattern from that observed for most other rivers. In the Guangli River, the distribution fluctuation was stronger than that in other TFR rivers. Reaches that flowed through urban areas had significantly higher truly dissolved Pb than reaches in the estuary and canal source. Low levels of truly dissolved Pb (less than 1.00 μg L^{-1}) were observed in the Shenxiangou River, except for SS5 (about 5.98 μg L^{-1}) at the estuary area. However, a sharp decrease (of about 5.60 μg L^{-1}) of truly dissolved Pb occurred with a salinity increase from ≈21.00 to ≈30.00. In general, truly dissolved Pb followed an obvious input and migration process in some areas. Furthermore, these processes are greatly disturbed by human activity.

3.3.3 Colloidal Pb

Colloidal Pb (>1 kDa) is Pb ions complexed with or adsorbed to colloidal matter, which has a relatively stronger bioavailability and chemical activity than other forms of dissolved lead. It is an important reservoir for Pb in natural water. The data of different sizes of colloidal Pb are detailed in Figure 5. As illustrated in the figure, colloidal Pb (>1 kDa) is the major constituent of the total dissolved Pb in the seaward rivers in the Yellow River Delta. A total of 46% of sample stations recorded high percentages (≈50.00%) of colloidal Pb. At the SX1 (on the Xiaoqinghe River), the percentage of the colloidal Pb even accounted for more than 95.00% of the total dissolved metal. Furthermore, there were only three stations that recorded low colloidal fractions below or around 10%: SX6, SG6, and SS5. In the sample stations near the estuary, colloidal Pb was higher, ranging from 41.52% to 86.94%.

In the natural river, the percentage of colloidal lead expressed a different distribution trend. In the Yellow River, most colloidal Pb was close to 40%. As shown in Figure 5A, the metal was mainly bound by the 1–3 kDa and 100 kDa–0.22μm colloidal matter, with values of ≈30.00% and ≈50.00%, in most of stations, respectively. Obvious changes occurred in low MWCO (1–100 kDa). At SY1, 1–3 kDa Pb (≈25.00% decrease) migrated into the 10–100kDa colloidal matter (≈23.00% increase). But at SY3, the percentage of 10–100 kDa Pb decreased to 0% and 3–10 kDa Pb increased from 0.74% to 23.78%, respectively. In the Xiaoqing River, those changes are much more complicated with the input of another river and salinity. As shown in Figure 5B, 1–3 kDa Pb was the main component (> 70.00%) before the input from the Zihe River in the Xiaoqing River. At the mixture station (SX4), the percentage of 1–3kDa Pb decreased to 5.74%, but 100 kDa–0.22 μm Pb and 3–10 kDa Pb increased from 9.71% to 40.16% and 14.39% to 36.07%, respectively. After the mixture, 10–100 kDa Pb was found in a low percentage (of about< 10.00%) and the distribution of colloidal Pb mainly occurred in 3 kDa–0.22 μm colloidal matter. Furthermore, Pb ions prefer to distribute to 3–10 kDa and 100 kDa–0.22 μm colloidal matter near the estuary.

An opposite distribution characteristic of colloidal lead was found in the trunk canals strongly influenced by seawater (SFR). The percentage of colloidal Pb in the Yongfenghe River increased continuously from 39.34% to 80.99% with the increase of salinity, but it gradually decreases from 71.85% to 52.45% in the Xiaodaohe River. There was no obvious relationship between the distribution of Pb in the different sizes of colloidal matter and salinity. Pb ions were still mainly bound by the 1–100 kDa colloidal matter, similar to its distribution characteristic in natural rivers (Figure 5C). In the Xiaodaohe River, which is more affected by seawater, colloidal Pb with a size of 100 kDa–0.22 μm was stable at about 41.00% ± 1.30% (Figure 5D). However, the percentage of 100 kDa–0.22 μm Pb changed significantly in the Yongfenghe River, which is weakly affected by seawater. This shows the obvious migration behaviors of Pb ions in different sizes of colloidal matter.

In the trunk canals weakly influenced by seawater (WFR), colloidal Pb presents various distribution characteristics with different rivers reaches. In the Zhimaihe River, the percentage of colloidal Pb exhibited a fluctuating reduction trend from 89.50% to 56.18% as the stations approached the estuary. A sharp decrease in concentration (from 35.88 μg L^{-1} to 1.28 μg L^{-1}) and the percentage (from 89.50% to 26.83%) of colloidal Pb was observed at the station where the seawater began to interact with freshwater (Figure 5E). The distribution of Pb in different sizes of colloidal matter changed from the 3–10 kDa fraction to the 10–100 kDa and 100k–0.22 μm fractions. Never the less, a significant increase in concentration (i.e., from 1.25 μg L^{-1} to 7.27 μg L^{-1}) and percentage (from 47.71% to 56.18%) of colloidal Pb occurred near the estuary (SZ5). The colloidal Pb mainly was in the 1–3 kDa fractionation at about 47.04% for this station. Differing from the Zhimai River, the Guangli River has a longer section that is not affected by salinity and that also passes through an urban area. The hydrodynamic force of this part of the river is relatively slow, and the interaction between colloidal matter and Pb is more sufficient. The concentration and percentage of colloidal Pb ranged from 0.68 μg L^{-1} to 5.46 μg L^{-1} and from 10.63% to 88.86%, respectively. The distribution of colloidal Pb changed from the 3–100 kDa fraction to the 100 kDa–0.22 μm fraction. Notably, in the station near the estuary, the salinity makes the distribution of Pb more uniform in the different sizes of colloidal matter (Figure 5F). Similar to the Guangli River, the Shenxiangou River also has a reach (SS1→SS4) less affected by seawater (Figure 5G). The concentration and percentage of colloidal Pb ranged from 0.99 μg L^{-1} to 5.88 μg L^{-1} and from 20.77% to 88.99%, respectively, in this area. In this area, colloidal Pb was also mainly distributed in fractions of 3–100 kDa to 100 kDa–0.22 μm. However, the percentage of colloidal Pb decreased to ≈10.00% with a significant increase in salinity. It should be noted that the percentage of colloidal Pb in the total

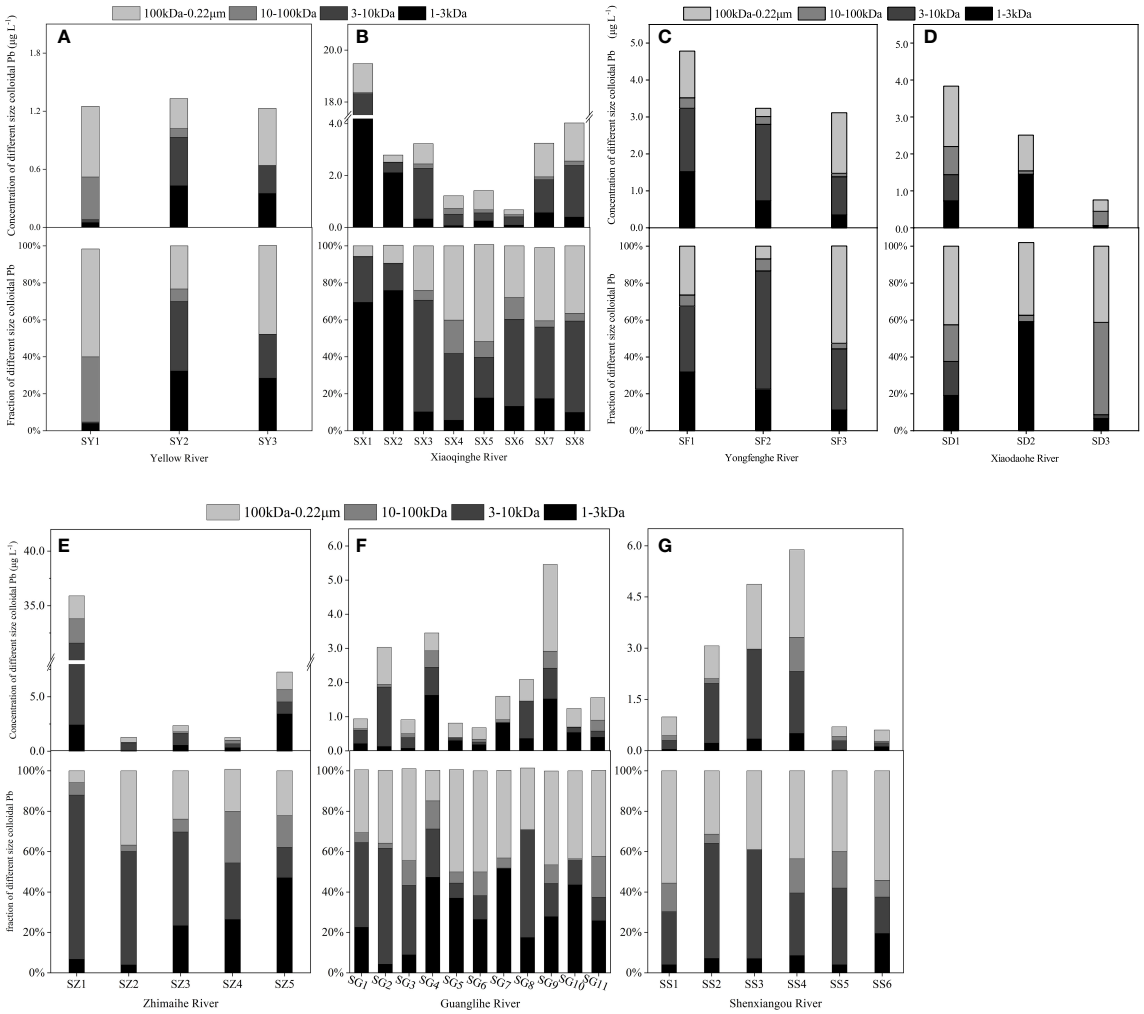

FIGURE 5
The concentration and fractionation of different sizes of colloidal lead (Pb). **(A)** The concentration and fractionation of different sizes of colloidal Pb in the Yellow River; **(B)** the concentration and fractionation of different sizes of colloidal Pb in the Xiaoqinghe River; **(C)** the concentration and fractionation of different sizes of colloidal Pb in the Yongfenghe River; **(D)** the concentration and fractionation of different sizes of colloidal Pb in the Xiaodaohe River; **(E)** the concentration and fractionation of different sizes of colloidal Pb in the Zhimaihe River; **(F)** the concentration and fractionation of different sizes of colloidal Pb in the Guanglihe River; and **(G)** the concentration and fractionation of different sizes of colloidal Pb in the Shenxiangou River.

dissolved metal increased significantly, but the actual concentration decreased. In all, salinity is an important factor that promotes the partitioning of Pb ions into 1–3 kDa and 100 kDa–0.22 μm fractions.

4 Discussion

4.1 The migration behavior of Pb

In this study, the migration behavior of Pb in the Yellow River was used as a reference location. This sample reach is not affected by industrial and domestic wastewater outfalls and agricultural activities in the winter. In addition, the concentration parameters showed that colloidal Pb (1.27 ± 0.06 μg L^{-1}) is basically stable in the Yellow River. This means that the Pb migration mainly occurs between the truly dissolved and particulate or sediment phase related to the weakened hydrodynamics. As the Yellow River flows into the sea, the main channel gradually becomes wider with a reduction in flow (Du et al., 2022). Low hydrodynamic action increases the chance of truly dissolved Pb entering the sediment with particle settlement (Moore et al., 1996). However, anthropogenic activities significantly influenced the Pb concentration behavior regarding partition patterns between colloid and truly dissolved Pb in other rivers. The change trend of the

fractionation factor (F) of Pb in the different phases is shown in Figure 6. The Xiaoqing River sampling area consisted of three reaches, the upper reach (SX1), the middle reach (SX2→SX6) and the estuary (SX7→SX8) (Figure 1). The upper reach and the estuary are greatly affected by chemical industry, salt industry, and port activities, whereas the middle reach is less affected by human activities because there is little agricultural activity in winter. Sewage discharge from the refining and chemical industry likely led to the surge of colloidal Pb (to 19.60 μg L^{-1}) at the SX1 station. Downstream in SX2, the colloidal Pb decreased sharply and truly dissolved Pb was stable. This phenomenon might be due to the unstable upstream chemical source of colloidal Pb, and input sources disappeared in this region (Teien et al., 2004). In addition, the colloidal Pb and truly dissolved Pb in the Xiaoqing River increased significantly after passing through some large residential areas (SX4). This phenomenon is related to the direct discharge of sewage from this area (Gu et al., 2022). Domestic wastewater produced by residential areas often contains large amounts of Pb and organic matter (Deng et al., 2020; Silva et al., 2020). In addition, this residential area is also home to petrochemical factories. The factories could produce wastewater containing high levels of Pb and organic matter (Wang et al., 2017; Dong et al., 2022). Hence, the domestic mixed factory discharge is likely to be an important source and disturbance factor of Pb in the Xiaoqing River. Notably, total dissolved Pb changed little after flowing through the area with less human influence (SX4→SX6). Furthermore, the dissolved Pb mainly migrated from the colloid phase to the truly dissolved phase (Figures 5, 6). This phenomenon is the opposite of the behavior of dissolved Pb in the Yellow River. It may be related to a difference of types of colloidal organic matter that are present in the Yellow River and the Xiaoqing River (Lu et al., 2021). An increase in colloidal Pb was observed after passing through the Yangkou port with its intensive human activities (SX8). The significant reduction of truly dissolved Pb in this region may be related to the rapid increase in salinity. Similar phenomena as were observed in the Xiaoqing River was also observed in the Zhimaihe River, the Yongfenghe River, and the Xiaodaohe River. Both the concentration and the fractionation of colloidal Pb significantly increased after those rivers passed through ports or residential areas (Figure 5). However, the migration of Pb was more complex in the Guanglihe River and Shenxiangou River because of the lower hydrodynamic force combined with the higher flow through urban areas. Previous studies have shown higher levels of Pb and more variable biogeochemical parameters, such as DOC and CDOM, in rivers flowing through urban areas (Liang et al., 2018; Liu et al., 2022). Overall, domestic and industrial sewage were the dominant factor regarding partitioning between truly dissolved Pb and colloidal Pb in the rivers flowing into the sea in the Yellow River Delta in the winter.

4.2 The roles of salinity, pH, and temperature

As shown in Figure 7, total dissolved Pb sharply decreased with salinity gradient, expect for the Zhimaihe River. It previously demonstrated that salinity could induce the flocculation of Pb in river water and this behavior was non-conservative (Wu et al., 2015). However, Pb in different phase express different behavior. Truly dissolved Pb gradually decreased with the salinity gradient and expresses a non-conservative behavior (Figure 7). But for colloidal Pb, both non-conservative and conservative behavior can be observed. The removal behavior of Pb mainly occurs in the truly dissolved

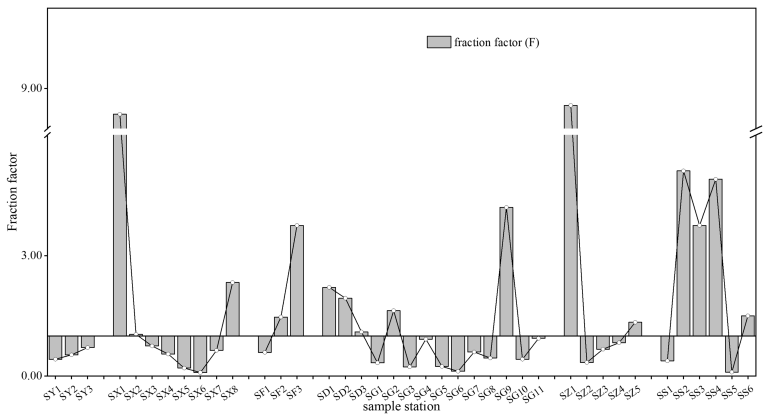

FIGURE 6
The fractionation factor (F) of lead (Pb_3) between the colloidal and truly dissolved phases. SY represents the Yellow River; SX represents the Xiaoqinghe River; SF represents the Yongfenghe River; SD represents the Xiaodaohe River; SZ represents the Zhimaihe River; SG represents the Guanglihe River; and SS represents the Shenxiangou River.

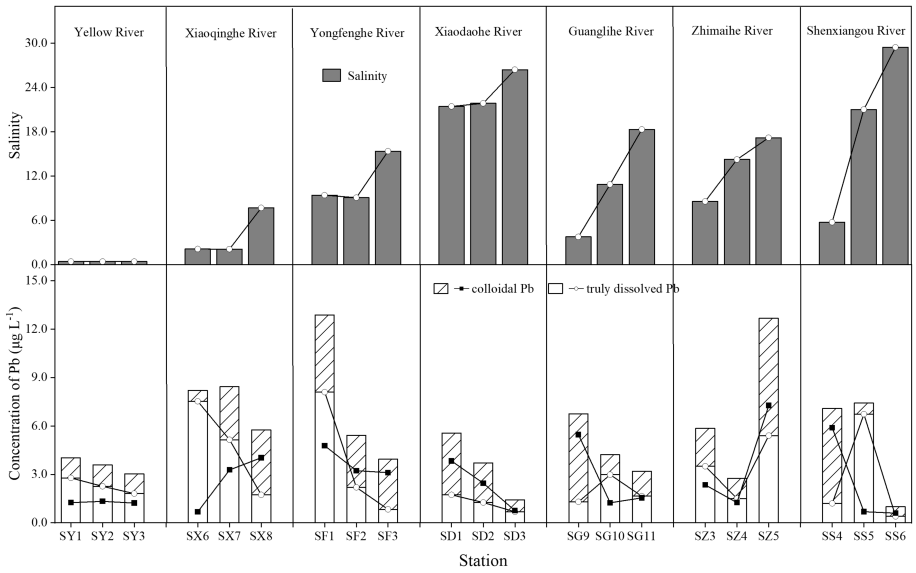

FIGURE 7
Changes in the trend of total dissolved lead (Pb) with the increase of salinity in different rivers.

state. This phenomenon may be the result of the combined effect of the speciation of Pb ions and the flocculation effect of salinity on low molecular organic matter (Xu et al., 2020; Nghiem et al., 2022). At elevated pH (>8.00), Pb ions easily transform to $PbCO_3$ precipitate with increasing of salinity (Powell et al., 2009). Some studies had demonstrated that organic Pb chelates was the dominate species in the truly dissolved Pb in natural water (Raudina et al., 2021). Therefore, the gradual increase in salinity and higher pH promotes the precipitation of truly dissolved Pb (Table 2). To clarify this combined effect, we performed principal component analysis of the pH and salinity variables with different state Pb and shown in Figure 8. From the figure we could found, pH values and salinity of the river water have similar negative correction with the dissolved Pb, especially for the truly dissolved Pb. But for colloidal Pb, pH expresses a positive correlation (Figure 8B). Meanwhile, pH had more intense effect than salinity for all state Pb (Figure 8). This behavior may dominate by the interaction between salinity, pH, and the accumulation of colloid matter (Cantwell and Burgess, 2001). Salt may induce organic matter to aggregate with each other for flocculation (Lasareva et al., 2019), but not completely flocculate the large sized colloidal matter (Herzog et al., 2019). The colloidal material can be stable under high pH and high salinity such as humic acid (Liu and Gao, 2019; Furukawa et al., 2014). The coagulation of inorganic colloids would reduce while above a certain salinity range, especially in presence of organic matter (Wang et al., 2015; Zhang et al., 2015). Therefore, temperature might another factor to affect the migration of Pb. It had demonstrated that temperature tended maintain the stabilization COC in the winter river (Gong et al., 2022). The principal component analysis between the temperature with different dissolved state Pb also performance (Figure 8). Low temperature had a positive correction with the state of dissolved Pb (Figure 8). It means temperature might an important factor to maintain the dissolve state of Pb. However, pH had a significant negative correction with the truly dissolved Pb (Figure 8C). It means truly dissolved Pb removal from the water in the estuary area where the salinity increasing rapidly, higher pH values, and especially in the low temperature. These results suggested that low temperature, high pH, and increased salinity have a combined or together effect on the removal of Pb form river water. These three biogeochemical factors associated reduced 33.3%≈95.4% of Pb entering to the sea with the seaward river.

4.3 The role of colloidal matter

Colloidal Pb was stable, and the colloidal organic carbon (COC, represented by the concentration of DOC) decreased with the direction toward the sea in the Yellow River (Figure S1). However, 10–100kDa colloidal Pb demonstrates a significant correlation with the change of COC (Table S1; Figure S1). This phenomenon might be related to the components of colloidal matter. It has demonstrated that different colloidal components could strongly bind the Pb_3 ions in water, and this binding ability varies with the character of the colloidal matter (Stolpe and Hassellov, 2010; Feng et al., 2022). However, it is difficult to clarify this effect because of the lack of analysis techniques that exactly separate and

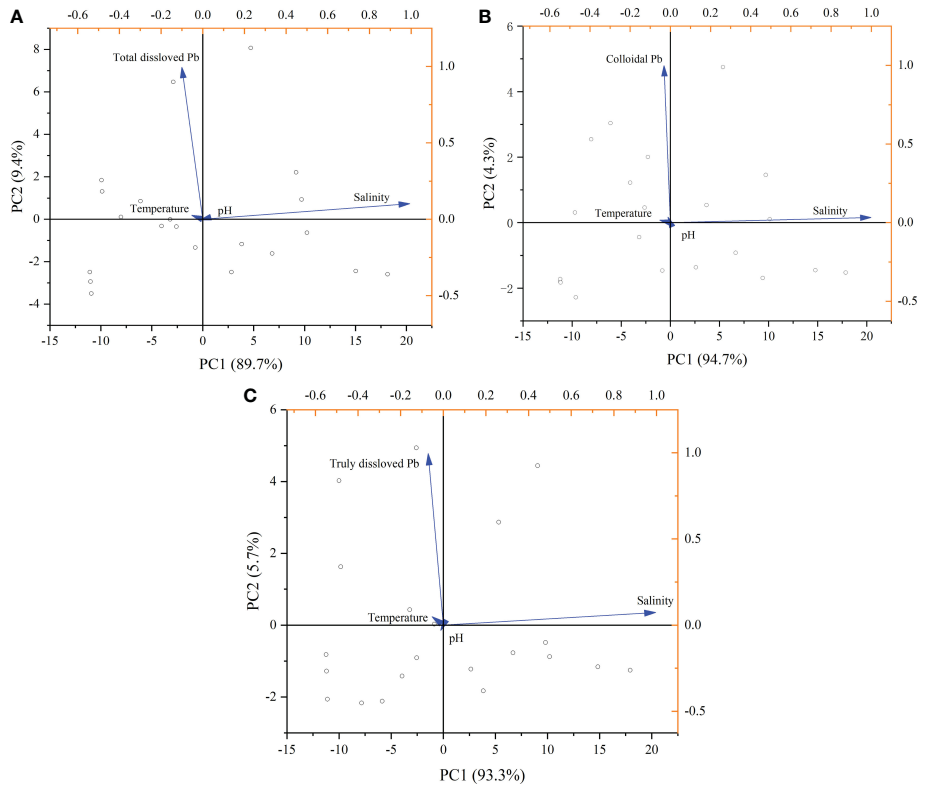

FIGURE 8
The principal component analysis of temperature, pH, and salinity with lead (Pb) at different dissolved states. **(A)** For total dissolved Pb; **(B)** for colloidal Pb; and **(C)** for truly dissolved Pb.

quantify colloidal matter components (Klun et al., 2019). Fortunately, some studies have discovered a significant relationship between CDOM of colloidal matter and Pb ions (Javed et al., 2017). Hence, we discussed the correlation between the molecular weight and components of CDOM and the colloidal Pb to explore this effect (Stolpe and Hassellov, 2010). The CDOM-UV parameter in different stations was shown in Table 3. We used the absorption constant at 355 nm to represent the concentration of CDOM, $SUVA_{254}$ represents the aromaticity of CDOM, and *a*250/*a*365 represents the molecular of CDOM.

In the Yellow River, the concentration of CDOM and COC was decreased but $SUVA_{254}$ was enhanced. Meanwhile, the *a*250/*a*365 value (10.09–14.45) showed that the molecular weight of CDOM was higher (Table 2). However, the concentration and the aromaticity of CDOM had a poor correlation with the different sizes of colloidal Pb (Figure S2). This shows that non-aromatic organic matter exhibited obvious aggregation or elimination, and inert soluble organic matter increased in concentration (Lu et al., 2019). In addition, Pb ions tend to partition in high-molecular-weight colloidal organic matter (Figure 5). Hence, the stable colloidal Pb in the Yellow River indicates a likely close relationship with this metal to the high-molecular-weight aromatic-like matter. Therefore, results suggest that the migration of colloidal Pb may be related to aromatic CDOM in areas with less disturbance from human activities and freshwater areas. In the Xiaoqing River, which is also a natural river, the changes of CDOM and colloidal Pb were more complicated. Except for the Zihe input station (SX4), the aromaticity and molecular weight of CDOM in the Xiaoqing River were lower (Table 2 and Figure S3). This illustrates that the distribution of Pb_3 in different sizes of colloidal matter have a close relationship with the high-molecular-weight aromatic matter. However, in the trunk channels which are greatly affected by the tide, the salinity induced the aromatic components of CDOM to gradually aggregate and promote agglomeration of colloidal Pb. Meanwhile, the trend in change of the CDOM abundance was conformation for all sizes of colloidal Pb (Figures S4–S8). Human activity mainly causes input of low-molecular-weight CDOM, which is also an important migration destination of Pb ions (Figure 5). The CDOMs are not stable and have relative ease of decomposition, inducing a complex distribution of Pb in different sizes of colloidal matter (Table 2). Overall, the highest concentration of colloidal Pb_3 was observed in the station that has stronger aromaticity of present CDOM

10.3389/fmars.2022.1085142

TABLE 3 The chromophoric dissolved organic matter (CDOM)-UV parameter in different sample stations.

Sample station	$a(355)$ (m^{-1})	$SUVA_{254}$	$a(250)/a(365)$
Yellow River			
SY1	0.47	3.11	10.09
SY2	0.52	4.04	14.45
SY3	0.23	8.46	10.32
Xiaoqinghe River			
SX1	0.93	0.3	3.98
SX2	3.47	0.25	1.43
SX3	5.41	3.13	3.37
SX4	1.9	3.82	9.45
SX5	4.67	1.2	2.51
SX6	4.06	1.42	0.78
SX7	2	2.38	1.6
SX8	3.95	1.36	4.75
Yongfenghe River			
SF1	3.77	0.92	5.12
SF2	1.72	5.28	9.66
SF3	0.86	3.87	2.89
Xiaodaohe River			
SD1	2.67	2.33	1.42
SD2	3.35	6	0.84
SD3	1.12	33.28	16.1
Zhimaihe River			
SZ1	4.35	10.01	0.79
SZ2	4.42	1.72	4.21
SZ3	3.89	1.88	0.93
SZ4	2.84	13.01	1.19
SZ5	4.67	15.29	0.63
Guanglihe River			
SG1	4.9	6.94	0.62
SG2	7.99	0.21	1
SG3	4.13	3.67	0.78
SG4	5.34	3.42	0.69
SG5	3.01	2.9	1.1
SG6	3.53	1.92	5.21
SG7	2.95	3.4	0.91
SG8	3.34	5.27	1.09

(Continued)

TABLE 3 Continued

Sample station	$a(355)$ (m^{-1})	$SUVA_{254}$	$a(250)/a(365)$
SG9	3.3	6.65	0.76
SG10	3.06	3.28	0.91
SG11	0.62	4.45	22.03
Shenxiangou River			
SS1	1.98	2.31	1.76
SS2	2.35	14.42	7.68
SS3	2.33	6.76	6.13
SS4	5.06	10.49	3.1
SS5	2.67	1.39	0.27
SS6	0.43	5.9	6.79

(Table 2 and Figure 5). Furthermore, Pb was also more inclined to be found in the large-sized colloidal matter. However, in winter, the distribution of Pb in large-sized colloids is relatively stable because of the low decomposition effect of the low temperature.

To further verify those findings, we compared the fractionation behavior between Pb in the truly dissolved phase and colloidal organic matter phase in other rivers into the sea. Table 4 shows the concentration of Pb in the truly dissolved phase and colloidal phase in different areas. It can be observed from Table 4 that the truly dissolved Pb was the main components in the freshwater (Javed et al., 2017; Gandois et al., 2020; Lu et al., 2020; Zhang et al., 2022). However, with the enhancement of salinity, the colloidal Pb became the main components of the dissolved Pb in the brackish water environment (Illuminati et al., 2019; Lu et al., 2020; Pavoni et al., 2020; Feng et al., 2022; Nasrabadi et al., 2022). Many studies have demonstrated that Pb is prone to sedimentation in estuary where salt water and freshwater are mixed (Pavoni et al, 2020; Nasrabadi et al., 2022). This phenomenon of migration distribution is more pronounced in the estuarine area. For example, colloidal Pb exceeded 50% of the total dissolved Pb in most estuarine areas (Illuminati et al., 2019; Lu et al., 2020; Pavoni et al., 2020; Feng et al., 2022; Nasrabadi et al., 2022). In the Krka River estuary, this fractionation behavior was close to 100% (Nasrabadi et al., 2022). Combined with the phenomenon of this study, the sedimentation of Pb mainly occurred in the small molecule organic phase (Figure 5). In addition, the increase in salinity promoted the migration of Pb to macromolecular colloids (Figures 5, 6). This suggests that macromolecular colloids matter will be the main dissolution state of Pb from rivers to the ocean.

TABLE 4 The concentration of lead (Pb_3) in the truly dissolved and colloidal phases in different river flows into the sea.

	River or estuary	Colloidal Pb	Truly dissolved Pb	References
Freshwater	Guandang River estuary	13%	87%	Lu et al., 2020
	Athabasca River	≈40%	≈60%	Javed et al., 2017
	Taihu Lake	≈34%	≈76%	Zhang et al., 2022
	Blackwater river	22%	78%	Gandois et al., 2020
	In this study	31–40%	60–69%	
Brackish water	Po River Estuary	≈70%	≈30%	Illuminati et al., 2019
	Guandang River estuary	58%	42%	Lu et al., 2020
	Pearl River Estuary	82%	18%	Fang et al., 2021
	Isonzo/Soča River mouth	84–95%	6%–15%	Pavoni et al., 2020
	Krka River estuary	99.00%	1.00%	Nasrabadi et al., 2022
	In this study	50–80%	20–50%	

4.4 Potential ecological effects of Pb

From the concentration change of Pb observed in this study, we could find that, excluding the influence of industrial pollution input, most Pb was precipitated in the estuary (Figure 7). This indicates that the ecological risk of Pb in the river water was relatively low. However, the disturbance by anthropogenic factors increases the risk of Pb migrating to the sea (Wang et al., 2022). As the winter passes, the strong hydrodynamic force caused by Yellow River flows will induce scouring of the trunk channel riverbed (Mistri et al., 2019). Pb deposited in surface sediments in winter will be carried into the sea by later floods. Furthermore, the water body replacement of the urban water system and river dredging works will periodically bring urban sedimentary Pb into the offshore environments. Meanwhile, these rivers do not have a strong hydrodynamic force and vast estuary areas like the natural Xiaoqing River and the Yellow River. Hence, trunk canals (Yongfenghe River and Xiaodaohe River) and urban water systems (Guanglihe River and Shenxiangou River) may be more likely to transport sedimentary Pb to the sea.

There will still a large amount of Pb transported into the sea with the river in the Yellow River Delta. Free Pb ions were easily precipitated in the water with multiple geochemical factors. However, the colloidal Pb after salinity selection at the estuary was more stable in seawater (Chambari et al., 2018). Colloidal Pb is also more easily taken up by organisms in the water because of its organic characteristics. The ecological risk of colloidal Pb was higher than Pb ions because of the easier enrichment of this speciation in the food chain (Lintner et al., 2019). In addition, mariculture, ports, and coastal factories have become the main sources of colloidal Pb. The wastewater discharged from these areas has high salinity. Colloidal Pb in that wastewater will go through a long time of salinity selection. For this, the sedimentation of colloidal Pb will become reduced at the estuary (Lee et al., 2014). A large amount of active Pb will directly input into the seawater, increasing ecological risks. Hence, the pollution by mariculture, ports, and coastal factories should require further attention to reduce ecological impacts.

5 Conclusions

Distribution and migration behavior of toxic metal Pb in the seaward river in the Yellow River Delta in winter was studied. The results showed that the discharge from factories and residential locations are important sources of Pb because the higher concentration of Pb in the reaches crossing urban areas. The migration of Pb in the river water phase was mainly dominated by the biogeochemical factors and the characteristics of COC. The rapidly increasing salinity and higher pH values, especially the low temperature, dominated the removal of Pb from the river water. Increasing salinity and pH induced the removal of truly dissolved Pb from the river. By the combined effect, 80% of Pb present precipitated and settled into the estuary, making this area a sink for Pb in winter. The fractionation results indicated that the specific components of colloidal organic matter were the key factor to driver the migration of Pb in colloidal phase. The drastic migration of Pb in different sizes of colloidal matter accompanied by obvious fluorescence and UV absorption intensity of CDOM increases and decreases. It is worth noting that colloidal Pb inputs from ports and mariculture are not prone to precipitate in the estuary area, which will enhance the ecological risks of this metal in near-shore environments.

In summary, the study results suggest that the change of pH and salinity stores a large amount of Pb in the trunk channel and estuary sediments in winter. Colloidal matter prevented this removal behavior and different sizes of colloids play different inhibitory roles. However, unfortunately, there is still a significant amount of information lacking. Further studies are needed to examine the interaction between Pb and the different sizes or chemical composition of COC.

Data availability statement

The original contributions presented in the study are included in the article/Supplementary Material. Further inquiries can be directed to the corresponding author.

Author contributions

PR and KL contributed to the conception, design, and investigation of the study; BS organized the database and performed the statistical analysis; and QL, SW, XL, and DS wrote sections of the manuscript. All authors contributed to manuscript revision, and read and approved the submitted version.

Funding

This study was funded by the National Key R&D Program of China under contract 2020YFD0900604; and the Conservation and restoration of bio-resources and habitats in typical coastal zones in Shandong province project under contract CF-MEEC/ER/2016–03.

Acknowledgments

We would like to thank Wen Chang and Bingchen Wang for their field and laboratory assistance, helpful advice, and in-depth discussion.

Conflict of interest

The authors declare that the research was conducted in the absence of any commercial or financial relationships that could be construed as a potential conflict of interest.

Publisher's note

All claims expressed in this article are solely those of the authors and do not necessarily represent those of their affiliated organizations, or those of the publisher, the editors and the reviewers. Any product that may be evaluated in this article, or claim that may be made by its manufacturer, is not guaranteed or endorsed by the publisher.

Supplementary material

The Supplementary Material for this article can be found online at: https://www.frontiersin.org/articles/10.3389/fmars.2022.1085142/full#supplementary-material

References

Abdelrady, A., Bachwenkizi, J., Sharma, S., Sefelnasr, A., and Kennedy, M. (2021). The fate of heavy metals during bank filtration: Effect of dissolved organic matter. *J. Water. Process. Eng.* 38, 101563. doi: 10.1016/j.jwpe.2020.101563

Cantwell, M. G., and Burgess, R. M. (2001). Metal-colloid partitioning in artificial interstitial waters of marine sediments: Influences of salinity, pH, and colloidal organic carbon concentration. *Environ. Toxicol. Chem.* 20, 2420–2427. doi: 10.1002/etc.5620201104

Cao, Q. Q., Wang, H., Li, Y. R., Zhang, Y. R., Zheng, P. M., Wang, R. Q., et al. (2018). The national distribution pattern and factors affecting heavy metals in sediments of water systems in china. *Soil. Sediment. Contam.* 27, 79–97. doi: 10.1080/15320383.2018.1424113

Chambari, S., Karbassi, A., Monavari, S. M., Sabzalipour, S., and Moattar, F. (2018). The role of estuarine natural flocculation process in the removal of heavy metals. *Fresen. Environ. Bull.* 27, 2468–2475.

Cheng, X. Y., Zhu, J. R., and Chen, S. L. (2021). Extensions of the river plume under various yellow river courses into the bohai Sea at different times. *Estuar. Coast. Shelf. S.* 249, 107092. doi: 10.1016/j.ecss.2020.107092

Chen, T., Wen, X. C., Zhang, L. J., Tu, S. C., Zhang, J. H., Sun, R. N., et al. (2022). The geochemical and mineralogical controls on the release characteristics of potentially toxic elements from lead/zinc (Pb/Zn) mine tailings. *Environ. pollut.* 315, 120328. doi: 10.1016/j.envpol.2022.120328

Dallas, L. J., Cheung, V. V., Fisher, A. S., and Jha, A. N. (2013). Relative sensitivity of two marine bivalves for detection of genotoxic and cytotoxic effects: a field assessment in the Tamar estuary, south West England. *Environ. Monit. Assess.* 185, 3397–3412. doi: 10.1007/s10661-012-2800-0

Deng, J. C., Zhang, J., Yin, H. B., Hu, W. P., Zhu, J. G., and Wang, X. L. (2020). Ecological risk assessment and source apportionment of metals in the surface sediments of river systems in lake taihu basin, China. *Environ. Sci. pollut. R.* 27, 25943–25955. doi: 10.1007/s11356-019-05719-5

Dong, W. P., Ci, M. W., Yan, X. S., Wang, Y. Q., Zhang, G. D., Xu, W. F., et al. (2022). Antibiotics in the surface water and sediment from the tributaries of the xiaoqing river, China: occurrence, distribution and risk assessment. *Desalin. Water. Treat.* 247, 229–243. doi: 10.5004/dwt.2022.28003

Du, X. K., Wang, K. R., Pei, H. Y., Dou, S. T., Bi, N. S., Zhang, X., et al. (2022). Geomorphic characteristics of the qingshuigou flow path in the yellow river estuary. *Mar. Sci.* 45, 77–85. doi: 10.11759/hykx20201213001

Fang, Q. S., Chen, Z. H., Zheng, J. P., and Zhu, Z. H. (2021). Comparison of Pb (II) and Cd(II) micro-interfacial adsorption on fine sediment in the pearl river basin, china. *Int. J. Sediment. Res.* 36, 401–418.

Feng, W. H., Wang, Z. F., Zhu, W. Z., Zheng, F. Q., Zhang, D. R., and Xu, H. T. (2022). Evaluation of the bioavailability of metals in sediment from the southern coastal wetland of the qiantang estuary by using diffusive gradients in thin films technique. *J. Ocean. U. China.* 21, 375–387.

Furukawa, Y., Reed, A. H., and Zhang, G. P. (2014). Effect of organic matter on estuarine flocculation: a laboratory study using montmorillonite, humic acid, xanthan gum, guar gum and natural estuarine floc. *Geochem. T.* 15, 1. doi: 10.1186/1467-4866-15-1

Fytianos, K. (2001). Speciation analysis of heavy metals in natural waters: A review. *J. Aoac. Int.* 84, 1763–1769. doi: 10.1093/jaoac/84.6.1763

Gandois, L., Hoyt, A. M., Mounier, S., Le Roux, G., Harvey, C. F., Claustres, A., et al. (2020). From canals to the coast: dissolved organic matter and trace metal composition in rivers draining degraded tropical peatlands in indonesia. *Biogeosciences* 17, 1897–1909.

Gao, X. L., Zhou, F. X., Chen, C. T. A., and Xing, Q. G. (2015). Trace metals in the suspended particulate matter of the yellow river (Huanghe) estuary: Concentrations, potential mobility, contamination assessment and the fluxes into the bohai Sea. *Cont. Shelf. Res.* 104, 25–36. doi: 10.1016/j.csr.2015.05.005

Gong, Y. Y., Bai, Y., Zhao, D. Y., and Wang, Q. L. (2022). Aggregation of carboxyl-modified polystyrene nanoplastics in water with aluminum chloride: Structural characterization and theoretical calculation. *Water. Res.* 208, 117884. doi: 10.1016/j.watres.2021.117884

Gu, X., Xin, M., Wang, J., Lu, S., Lian, M. S., Lin, C. Y., et al. (2022). Quantitative source identification and environmental assessment of trace elements in the water and sediment of rivers flowing into laizhou bay, bohai Sea. *Mar. pollut. Bull.* 174, 113313. doi: 10.1016/j.marpolbul.2021.113313

Guzman, E., Santini, E., Benedetti, A., Ravera, F., Ferrari, M., and Liggieri, L. (2014). Surfactant induced complex formation and their effects on the interfacial properties of seawater. *Colloid. Surface. B.* 123, 701–709.

Hargreaves, A. J., Vale, P., Whelan, J., Alibardi, L., Constantino, C., Dotro, G., et al. (2018). Impacts of coagulation–flocculation treatment on the size distribution and bioavailability of trace metals (Cu, Pb, Ni, zn) in municipal wastewater. *Water. Res.* 128, 120–128. doi: 10.1016/j.watres.2017.10.050

Herzog, S. D., Gentile, L., Olsson, U., Persson, P., and Kritzberg, E. S. (2019). Characterization of iron and organic carbon colloids in boreal rivers and their fate at high salinity. *J. Geophys. Res-Biogeo.* 125, e2019JG005517. doi: 10.1029/2019JG005517

He, D., Shi, X. M., and Wu, D. Y. (2016). Particle–size distribution characteristics and pollution of heavy metals in the surface sediments of kuitun river in xinjiang, China. *Environ. Earth. Sci.* 75, 104. doi: 10.1007/s12665-015-4882-9

Huang, H. J., Yuan, X. Z., Zeng, G. M., Zhu, H. N., Li, H., Liu, Z. F., et al. (2011). Quantitative evaluation of heavy metals' pollution hazards in liquefaction residues of sewage sludge. *Bioresource. Technol.* 102, 10346–10351. doi: 10.1016/j.biortech.2011.08.117

Illuminati, S., Annibaldi, A., Truzzi, C., Tercier–Waeber, M. L., Noel, S., Braungardt, C. B., et al. (2019). Scarponi, G in–situ trace metal (Cd, Pb, Cu) speciation along the po river plume (Northern Adriatic Sea) using submersible systems. *Mar. Chem.* 212, 47–63. doi: 10.1016/j.marchem.2019.04.001

Javed, M. B., Cuss, C. W., Grant-Weaver, I., and Shotyk, W. (2017). Size-resolved pb distribution in the athabasca river shows snowmelt in the bituminous sands region an insignificant source of dissolved pb. *Sci. Rep-UK.* 7, 43622.

Klun, K., Falnoga, I., Mazej, D., Sket, P., and Faganeli, J. (2019). Colloidal organic matter and metal(loid)s in coastal waters (Gulf of Trieste, northern Adriatic Sea). *Aquat. Geochem.* 25, 179–194. doi: 10.1007/s10498-019-09359-6

Lasareva, E. V., Parfenova, A. M., Romankevich, E. A., Lobus, N. V., and Drozdova, A. N. (2019). Organic matter and mineral interactions modulate flocculation across Arctic river mixing zones. *J. Geophys. Res-Biogeo.* 124, 1651–1664. doi: 10.1029/2019JG005026

Latosinska, J., and Czapik, P. (2020). The ecological risk assessment and the chemical speciation of heavy metals in ash after the incineration of municipal sewage sludge. *Sustainability.* 12, 6517. doi: 10.3390/su12166517

Lao, Q. B., Cai, S. J., Huang, P., Chen, F. J., Su, Q. Z., Lei, X. T., et al. (2022). Contaminant characteristics and influencing factors of heavy metals in seawater and sediments in a typical mariculture bay in south china. *Front. Mar. Sci.* 9, 923494.

Lao, Q. B., Su, Q. Z., Liu, G. Q., Shen, Y. L., Chen, F. J., Lei, X. T., et al. (2019). Spatial distribution of and historical changes in heavy metals in the surface seawater and sediments of the beibu gulf, china. *Mar. pollut. Bull.* 146, 427–434.

Lee, G. J., Son, H. A., Cho, J. W., Choi, S. K., Kim, H. T., Kim, J. W., et al. (2014). Stabilization of pickering emulsions by generating complex colloidal layers at liquid-liquid interfaces. *J. Colloid. Interf. Sci.* 413, 100–105. doi: 10.1016/j.jcis.2013.09.015

Liang, M. Q., Shao, M. L., Cao, C. L., Zong, Y. N., and Tang, J. F. (2018). Characteristics of dissolved organic matter (DOM) and relationship with dissolved heavy metals in a peri–urban and an urban river. *Environ. Sci.* 39, 2095–2103. doi: 10.13227/j.hjkx.201710089

Li, L., Liu, J., Wang, X., and Shi, X. (2015). Dissolved trace metal distributions and Cu speciation in the southern bohai Sea, China. *Mar. Chem.* 172, 34–45. doi: 10.1016/j.marchem.2015.03.002

Lintner, M., Lintner, B., Wanek, W., Keul, N., von der Kammer, F., Hofmann, T., et al. (2019). Effects of heavy elements (Pb, Cu, zn) on algal food uptake by elphidium excavatum (Foraminifera). *Heliyon.* 7, e08427. doi: 10.1016/j.heliyon.2021.e08427

Lin, W. N., Wang, N., and Fu, Q. (2019). Research on the pollutant bearing capacity of bohai sea under vater exchange. *Transac. Oceanol. Limnol.* 5, 42–48. doi: 10.13984/j.cnki.cn37-1141.2019.05.005

Liu, K., and Gao, X. L. (2019). Adsorption and fractionation of pt, pd and Rh onto inorganic microparticles and the effects of macromolecular organic compounds in seawater. *Environ. pollut.* 255, 113192. doi: 10.1016/j.envpol.2019.113192

Liu, K., Gao, X. L., Li, L., Chen, C. T. A., and Xing, Q. G. (2018). Determination of ultra–trace pt, pd and Rh in seawater using an off–line pre–concentration method and inductively coupled plasma mass spectrometry. *Chemosphere.* 212, 429–437. doi: 10.1016/j.chemosphere.2018.08.098

Liu, F., Liu, X. H., Zhao, S. N., Wang, J., and Qian, X. (2019). Photochemical transformations of tetracycline antibiotics influenced by natural colloidal particles: Kinetics, factor effects and mechanisms. *Chemosphere.* 235, 867–875. doi: 10.1016/j.chemosphere.2019.06.201

Liu, W. H., Ma, T., Du, Y., Wu, X. C., Chen, L. Z., Li, J. Q., et al. (2022). Characteristics of dissolved organic matter in surface water and sediment and its ecological indication in a typical mining–affected river–le'an river, China. *Environ. Sci. pollut. R.* 29, 37115–37128. doi: 10.1007/s11356-021-18478-z

Lu, Y. X., Gao, X. L., and Chen, C. T. A. (2019). Separation and determination of colloidal trace metals in seawater by cross–flow ultrafiltration, liquid–liquid extraction and ICP–MS. *Mar. Chem.* 215, 103685. doi: 10.1016/j.marchem.2019.103685

Lu, Y. X., Gao, X. L., Song, J. M., Chen, C. T. A., and Chu, J. L. (2020). Colloidal toxic trace metals in urban riverine and estuarine waters of yantai city, southern coast of north yellow Sea. *Sci. Total. Environ.* 717, 135265. doi: 10.1016/j.scitotenv.2019.135265

Lu, Y. X., Pan, D. W., Yang, T. T., and Wang, C. C. (2021). Spatial and environmental characteristics of colloidal trace Cu in the surface water of the yellow river estuary, China. *Mar. pollut. Bull.* 168, 112401. doi: 10.1016/j.marpolbul.2021.112401

Ma, T. T., Li, X. W., Bai, J. H., and Cui, B. S. (2019). Tracking three decades of land use and land cover transformation trajectories in china's large river deltas. *Land. Degrad. Dev.* 30, 799–810. doi: 10.1002/ldr.3268

Marcinek, S., Cindric, A. M., Padan, J., and Omanovic, D. (2022). Trace metal partitioning in the salinity gradient of the highly stratified estuary: A case study in the krka river estuary (Croatia). *Appl. Sci-Basel.* 12, 12.

Men, C., Liu, R. M., Xu, L. B., Wang, Q. R., Guo, L. J., Miao, Y. X., et al. (2020). Source–specific ecological risk analysis and critical source identification of heavy metals in road dust in Beijing, China. *J. Hazard. Mater.* 388, 121763. doi: 10.1016/j.jhazmat.2019.121763

Mistri, M., Pitacco, V., Granata, T., Moruzzi, L., and Munari, C. (2019). When the levee breaks: Effects of flood on offshore water contamination and benthic community in the Mediterranean (Ionian Sea). *Mar. pollut. Bull.* 140, 588–596. doi: 10.1016/j.marpolbul.2019.02.005

Moore, W. S., DeMaster, D. J., Smoak, J. M., McKee, B. A., and Swarzenski, P. W.. (1996). Radionuclide tracers of sediment–water interactions on the Amazon shelf. *Cont. Shelf. Res.* 16, 645–665. doi: 10.1016/0278-4343(95)00049-6

Mudge, M. C., Nunn, B. L., Firth, E., Ewert, M., Hales, K., et al. (2021). Subzero, saline incubations of colwellia psychrerythraea reveal strategies and biomarkers for sustained life in extreme icy environments. *Environ. Microbiol.* 23, 3840–3866. doi: 10.1111/1462-2920.15485

Nadella, S. R., Tellis, M., Diamond, R., Smith, S., Bianchini, A., Wood, C. M., et al. (2013). Toxicity of lead and zinc to developing mussel and sea urchin embryos: Critical tissue residues and effects of dissolved organic matter and salinity. *Comp. Biochem. Phys. C.* 158, 72–83. doi: 10.1016/j.cbpc.2013.04.004

Nghiem, J. A., Fischer, W. W., Li, G. K., Lamb, M. P., et al. (2022). A mechanistic model for mud flocculation in freshwater rivers. *J. Geophys. Res–earth.* 127, e2021JF006392. doi: 10.1029/2021JF006392

Nasrabadi, T., Soodarjani, A. E., Karbassi, A., and Baghdadi, M. (2022). Role of salinity and aeration on flocculation and remobilization of metals during estuarine mixing. *Environ. Earth. Sci.* 81, 277.

Pavoni, E., Crosera, M., Petranich, E., Oliveri, P., Klun, K., Faganeli, J., et al. (2020). Trace elements in the estuarine systems of the gulf of Trieste (northern Adriatic sea): A chemometric approach to depict partitioning and behavior of particulate, colloidal and truly dissolved fractions. *Chemosphere.* 252, 126517. doi: 10.1016/j.chemosphere.2020.126517

Peuravuori, J., and Pihlaja, K. (1997). Molecular size distribution and spectroscopic properties of aquatic humic substances. *Anal. Chim. Acta* 337, 133–149. doi: 10.1016/S0003-2670(96)00412-6

Powell, K. J., Brown, P. L., Byrne, R. H., Gajda, T., Hefter, G., Leuz, A. K., et al. (2009). Chemical speciation of environmentally significant metals with inorganic ligands. part 3: The Pb^{2+}, OH^-, cl^-, CO_3^{2-}, SO_4^{2-}, and PO_4^{3-} systems (IUPAC technical report). *Pure. Appl. Chem.* 81, 2425–2476. doi: 10.1351/PAC-REP-09-03-05

Raudina, T. V., Loiko, S. V., Kuzmina, D. M., Shirokova, L. S., Kulizhskiy, S. P., Golovatskaya, E. A., et al (1997). Colloidal organic carbon and trace elements in peat porewaters across a permafrost gradient in Western Siberia. *Geoderma* 390, 114971.

Savenko, A. V., and Savenko, V. S. (2019). Effect of natural organic acids on mobilization of macro– and microelements from rocks. *Dokl. Earth. Sci.* 485, 331–335. doi: 10.1134/S1028334X19030334

Silva, D. S., Cerqueira, U. M. F. M., Aguiar, R. M., Carneiro, P. L. S., and Bezerra, M. A. (2020). Characterization, fractionation and mobility of trace elements in surface sediments of the jequiezinho river, bahia, brazi. *An. Acad. Bras. Cienc.* 92, e20190558. doi: 10.1590/0001-3765202020190558

Stolpe, B., and Hassellov, M. (2010). Nanofibrils and other colloidal biopolymers binding trace elements in coastal seawater: Significance for variations in element size distributions. *Limnol. Oceanogr.* 55, 187–202. doi: 10.4319/lo.2010.55.1.0187

Teien, H. C., Salbu, B., Kroglund, F., and Rosseland, B. O. (2004). Transformation of positively charged aluminium–species in unstable mixing zones following liming. *Sci. Total. Environ.* 330, 217–232. doi: 10.1016/j.scitotenv.2004.03.040

Wang, X., Ren, L. J., Jiao, F. C., and Liu, W. J. (2017). The ecological risk assessment and suggestions on heavy metals in river sediments of jinan. *Water. Sci. Technol.* 76, 2177–2187. doi: 10.2166/wst.2017.380

Wang, L. F., Wang, X. F., Chen, H. G., Wang, Z. H., and Jia, X. P. (2022). Oyster arsenic, cadmium, copper, mercury, lead and zinc levels in the northern south China Sea: long-term spatiotemporal distributions, combined effects, and risk assessment to human health. *Environ. Sci. pollut. R.* 29, 12706–12719. doi: 10.1007/s11356-021-18150-6

Wang, S. S., Zhang, L., Yan, B., Xu, H. L., Liu, Q. X., and Zeng, H. B. (2015). Molecular and surface interactions between polymer flocculant chitosan-g-polyacrylamide and kaolinite particles: impact of salinity. *J. Phys. Chem. C.* 119, 7327–7339. doi: 10.1021/acs.jpcc.5b00739

Weng, H. X., Ma, X. W., Fu, F. X., Zhang, J. J., Liu, Z., Tian, L. X., et al. (2014). Transformation of heavy metal speciation during sludge drying: Mechanistic insights. *J. Hazard. Mater.* 265, 96–103. doi: 10.1016/j.jhazmat.2013.11.051

Wood, C. M., Al-Reasi, H. A., and Smith, D. S. (2011). The two faces of DOC. *Aquat. Toxicol.* 105, 3–8. doi: 10.1016/j.aquatox.2011.03.007

Worms, I. A. M., Slaveykova, V. I., and Wilkinson, K. J. (2015). Lead bioavailability to freshwater microalgae in the presence of dissolved organic matter: Contrasting effect of model humic substances and marsh water fractions obtained by ultrafiltration. *Aquat. Geochem.* 21, 217–230. doi: 10.1007/s10498-015-9256-0

Wu, J., Lu, J., Zhang, C., Zhang, Y. X., Lin, Y. C., and Xu, J. (2020). Pollution, sources, and risks of heavy metals in coastal waters of China. *Hum. Ecol. Risk. Assess.* 26, 2011–2026. doi: 10.1080/10807039.2019.1634466

Wu, G. H., Pan, L., Wei, Q., and Guo, L. (2015). Decreased mobility of heavy metals in haihe river sediments: The possible role of tide gate. *J. Geochem. Explor.* 157, 92–99. doi: 10.1016/j.gexplo.2015.06.002

Wu, W. G., Zhang, J. H., Liu, Y., Wang, X. M., Yang, J., and Feng, X. (2022) Spectral and distribution characteristics of colored dissolved organic matter (CDOM) in sanggou bay in spring. *J. Fish. China.*. doi: 10.11964/jfc. 20210813009

Xiang, M. T., Li, Y., Yang, J. Y., Lei, K. G., Li, Y., Li, F., et al. (2021). Heavy metal contamination risk assessment and correlation analysis of heavy metal contents in soil and crops. *Environ. pollut.* 278, 116911. doi: 10.1016/j.envpol.2021.116911

Xie, X. F., Pu, L. J., Zhu, M., Xu, Y., and Wang, X. H. (2019). Linkage between soil salinization indicators and physicochemical properties in a long-term intensive agricultural coastal reclamation area, Eastern China. *J. Soil Sediment.* 19 (11), 3699–3707. doi: 10.1007/s11368-019-02333-3

Xu, W., Gao, Q., He, C., Shi, Q., Hou, Z. Q., and Zhao, H. Z. (2020). Using ESI FT–ICR MS to characterize dissolved organic matter in salt lakes with different salinity. *Environ. Sci. Technol.* 54, 12929–12937. doi: 10.1021/acs.est.0c01681

Xu, H. C., Yan, M. Q., Li, W. T., Jiang, H. L., and Guo, L. D. (2018). Dissolved organic matter binding with Pb(II) as characterized by differential spectra and 2D UV-FTIR heterospectral correlation analysis. *Water Res.* 144, 435–443. doi: 10.1016/j.watres.2018.07.062

Zang, Z. F., Li, Y. H., Li, H. R., Guo, Z. H., and Zhang, R. (2020). Spatiotemporal variation and pollution assessment of Pb/Zn from smelting activities in China. *Environ. pollut.* 6, 1986. doi: 10.3390/ijerph17061968

Zhang, W. G., Feng, H., Qu, J. N., and Yu, L. Z. (2008). Lead (Pb) isotopes as a tracer of Pb origin in Yangtze river intertidal zone. *Chem. Geol.* 257, 260–266. doi: 10.1016/j.chemgeo.2008.10.012

Zhang, J., Wang, K., Yi, Q. T., Zhang, T., Shi, W. Q., and Zhou, X. F. (2022). Transport and partitioning of metals in river networks of a plain area with sedimentary resuspension and implications for downstream lakes. *Environ. pollut.* 294, 11868. doi: 10.1016/j.envpol.2021.118668

Zhang, J. F., Zhang, Q. H., and Qiao, G. Q. (2015). Effects of salinity on the flocculation of illite due to differential settling. *J. Hydrau. Engin.* 46, 1305–1311. doi: 10.13243/j.cnki.slxb.20150012

Zhi, L. H., Li, X. W., Bai, J. H., and Guan, Y. N. (2020). Integrating ecological and socioeconomic networks using nitrogen metabolism in the yellow river delta, China. *Resour. Conserv. Recy.* 162, 105012. doi: 10.1016/j.resconrec.2020.105012